Demonstrating single- and multiple currents through the *E. coli*-SecYEG-pore: Testing for the number of modes of noisy observations

Fadoua Balabdaoui[1], Kathrin Bissantz[2], Nicolai Bissantz[3] and Hajo Holzmann[4],

[1] CEREMADE, Université de Paris-Dauphine, France

[2] Institut für Medizinische Physik und Biophysik, Universität Münster, Germany

[3] Fakultät für Mathematik, Ruhr-Universität Bochum, Germany

[4] Fachbereich Mathematik und Informatik, Philipps-Universität Marburg, Germany

Abstract

We analyze a new dataset from a recording of transmembrane currents through a bacterial membrane channel to demonstrate the existence of single and multiple channel currents. Protein channels mediate transport through biological membranes; knowledge of the channel properties gained from electrophysiological recordings is important for a targeted drug design. We investigate the bacterial membrane protein SecYEG which is of essential importance for the secretory pathway for sorting of newly synthesized proteins to their place of function in the cell. Our results strongly indicate that in the SecYEG pore the different modes of the density of channel currents are approximately equidistant and correspond to different numbers of open channels in the membrane. A current of $\approx 12pA$ under the present experimental conditions turns out to be characteristic of the presence of a single open SecYEG pore, a fact that had not been electrophysiologically characterized so

far. Electrophysiological recordings of single protein channels show a substantial amount of background noise. The data at our disposal can be modeled as the independent sum of an error variable and the realization of the ionic current. Thus, we are led to deconvoluting the density of the observations in order to recover the density f of the ionic currents, and then investigating the number of modes of f. To this end we propose an extension of Silverman's (1981) test for the number of modes to deconvolution kernel density estimation, and develop the relevant theory. The finite sample performance of the test is investigated in a simulation study.

Keywords: bandwidth, bootstrap, deconvolution, kernel method, nonparametric density estimation, mode, electrophysiology, membrane pore protein, single channel current

AMS subject classification: Primary 62G15; Secondary 62G07.

1 Introduction

The cytoplasm of eukaryotic cells is separated from the aqueous extracellular space by the cell membrane, a lipid bilayer that is impermeable for small charged molecules such as ions and water. The exchange of substrate between cytoplasm and the extracellular space is facilitated by proteinaceous membrane spanning channels. There is a variety of these channel proteins specifically transporting substrates of different sizes and charge properties. The size of the central channel pore, the surface charge inside the pore and the transport mechanisms are adjusted to the different kinds of substrate.

Electrophysiology is the method of choice to explore the transport characteristics of transmembrane channels. It offers the possibility to observe the behaviour of

single channel proteins in a model membrane. Such electrophysiological recordings provide detailed insight into the transport dynamics of the pore which is important to exploit the channel properties e.g. for transport of pharmacological active substrates into the cell. Due to their high sensitivity, electrophysiological methods are applied for example to model the transport of pharmacological compounds such as antibiotics LIT across membranes (e.g. Nestorovich et al., 2002, Neves et al., 2005, and Danelon et al., 2006).

In the present experiment the electrophysiological properties of the bacterial membrane protein SecYEG were addressed. The SecYEG complex is the bacterial homologue of the mammalian Sec61 complex which is of essential importance for the secretory pathway for sorting of newly synthesized proteins to their place of function in the cell (cf. Lodish et al., 2000, Chapter 17.4: Transport of secretory proteins through the endoplasmatic reticulum [ER] membrane). Interactions between amino acid motifs (e.g. transmembrane motifs) of the nascent protein chain and the environment in the SecYEG pore play an important role for deciding if a protein is either translocated into the ER lumen or inserted into the ER membrane. This secretory pathway is of vital importance for the functionality of a cell; there are several diseases linked to defects in protein sorting and trafficking, e.g. Huntington's disease (cf. Caviston & Holzbaur, 2009) or Alzheimer's disease (cf. Yao et al. 2003).

The electrophysiological experiment now serves to characterize the properties of the inner SecYEG protein pore: The specific current levels, and the distance between them, give information on the size of the pore, its surface charge and the number of open channels in the membrane. To acquire recordings of a single protein channel, a model lipid membrane containing native *E.coli*-phospholipid is constructed by separating two electrolyte filled compartments by an artificial lipid membrane. Then, a constant voltage is applied across the membrane. Upon insertion of a channel

protein into the membrane a small current occurs that is amplified and digitally recorded.

The current levels acquired in the current signal are characteristic for the ion pore. In this paper we analyze the modality of the density f of these attained current levels. Note that we do not analyze the modality of the signal given by the measured current in dependence of time, but rather the modality of the levels to which the current jumps. Thus, in our analysis we consider those levels as an i.i.d. sample from the density under investigation.

The biological model under consideration is that the ion pore shows a reproducable and repeatable behavior with a characteristic, stable current level, depending on the voltage applied and the kind and concentration of ions in the solution where the membrane is embedded. The fixed current level would show up as a main peak in the current level distribution with potential additional modes at multiples of the main peak. In this paper, the model of a fixed current level will be tested against the null model of a strongly varying level, which would not yield a multimodal structure, but rather a single broad mode or a distribution that is monotonically decreasing.

An important characteristic of the electrophysiological data considered here is that the recording of single channel currents in artificial lipid bilayers is in general prone to high background noise. The measurements are very sensitive to electrical noise and also to the system intrinsic noise, e.g. from the electrodes and the electrolyte solution. To characterize membrane proteins with unknown transport properties it is essential to be able to distinguish a statistically significant signal and additional modes of the signal from noise of the estimated density.

In this setting, we are led to a measurement error problem, in which we have to do inference about the number of modes of the density f which is only observed with noise, thus resulting in an observed density g. To this end we shall use nonpara-

metric deconvolution kernel density estimation techniques, and extend Silverman's (1981) testing methodology for the number of modes to this setup.

Silverman (1981, 1983) observed that for fixed, non-noisy observations the number of modes in a kernel density estimate with the normal kernel is a monotonically decreasing function of the bandwidth. Using this fact Silverman (1981) defined the m-critical bandwidth h_m as the minimal bandwidth for which the kernel estimate still admits m modes, i.e. for which the estimate is just on the boundary between m and $m+1$ modes. Intuitively, if h_m is large, then a lot of smoothing is needed so that the density estimate only has m modes, which can be taken as an indication that the underlying density might in fact have more than m modes. More formally, if h_m exceeds a bootstrap critical value based on the smoothed bootstrap, the hypothesis for at most m modes of the underlying density is rejected in favor of the alternative of having more than m modes. Silverman's (1981) test has been further investigated in a number of papers, including those by Mammen et al. (1992), Cheng and Hall (1999) and Hall and York (2001). While inference on the number of modes of a nonparametric estimate is quite well studied for direct estimation problems, there seem to be no methods available yet for data which are observed with measurement error, thus leading to density deconvolution. Here, the formal setting is as follows. Let $X_1, \ldots, X_n$ be i.i.d. observations from the model

$$X_i = Z_i + \epsilon_i, \tag{1}$$

where we assume that the ϵ_i are i.i.d. with density ψ and independent of the Z_i. The object of interest is the density f of the Z_i, which is related to the density g of the X_i via $g = f * \psi$, the convolution of f and ψ. Recovering f from the noisy observations $X_1, \ldots, X_n$ is therefore called the deconvolution problem (e.g. Carroll and Hall 1988, Stefanski and Carroll 1990, Fan 1991a/b or Butucea and Matias 2005). Evidently, choosing a proper model $\hat{\psi}$ for the error density ψ is a relevant

problem in this context. For theoretical purposes, ψ is often assumed to be known (i.e. $\hat{\psi} = \psi$), but in any application it has to be empirically specified. In our application where additional data on the noise distribution is available, ψ can be estimated either parametrically or also nonparametrically.

A popular class of estimators for f in the deconvolution problem are kernel estimators $\hat{f}_n$. Here, one often uses a kernel L for which the Fourier transform is compactly supported in order to guarantee that $\hat{f}_n$ is well-defined for all bandwidths and all types of (sufficiently regular) error densities. However, we shall show that for most error densities, $\hat{f}_n$ is also well-defined if the normal kernel is employed and that the number of modes is monotonically decreasing in the bandwidth h as well.

Based on this observation, we discuss in Section 3 Silverman's (1981) test for deconvolution. However, the main purpose of this paper is the subsequent application of the proposed methodology to our new dataset from a recording of transmembrane currents through the bacterial membrane pore protein SecYEG. Hence, the paper starts in Section 2 with an introduction to the experimental setting.

In Section 4, a graphical analysis of the density estimates of current heights in the ionic fluxes with critical bandwidths for one, two and three modes is used to illustrate that the first and second, and the second and third peak, are separated by $\approx 12pA$, i.e. are approximately equidistant.

Using the calibrated Silverman's test for deconvolution we can show at an error level of 5% that these peaks are not mere sampling artifacts but rather are actual features of the underlying density f. Thus, in contrast to existing methods on peak-estimation, our approach allows to statistically assess the existence of modes. Further, in contrast to mere estimation, for obtaining valid p-values it is essential to take into account the additional observational errors ϵ_i. For the data, we conclude that peaks are linked to single and multiple channel currents.

Section 5 contains an extensive simulation study, and in Section 6 we conclude with a discussion. Some asymptotic theory for our methods is given in the Appendix. Proofs of the results are given in the companion technical report Balabdaoui et al. (2009).

2 Distribution of ionic fluxes through bacterial membrane pores

2.1 Experimental setup

Lipid membranes form impermeable barriers that separate a cell or an intracellular compartment from its surrounding aequeous environment. Transport of watersoluble substrates such as ions or small organic molecules across the membrane is facilitated by proteinaceous pores in the membrane. Ion flux through such membrane channel proteins is measured by electrophysiology. However, in-vivo analysis of the functionality of a specific membrane pore of a cell is impossible due to the large number of different pores present in a cell membrane which yield an unspecific signal in electrophysiological recordings. In contrast, in-vitro experiments allow for a targeted assessment of the behaviour of a single pore. Therefore, isolated protein channels are inserted into an artificial lipid membrane spanning a small aperture of approximately $50\mu m$ between two electrolyte filled chambers. A constant voltage is applied across the membrane serving as an isolator between the two compartments. Channel proteins are inserted into the artificial lipid membrane by fusion of protein containing liposomes with the membrane. Upon insertion of a protein pore into the membrane a transmembrane current occurs and is recorded (cf. Hemmler et al., 2005, Danelon et al., 2006). This method allows the detection of single

channel currents lying in the pico-Ampere [pA] range. The height of the different levels attained by the current signal gives information about the properties of the channel pore such as size and surface charge, and depends on the ionic strength of the solution. Important for the function of the protein is its correct folding (i.e. its geometric shape) into the membrane. This is identical for the native and artificial membrane, since the experimental membrane contains proteins that are also present in the native environment of the protein pore. Hence, electrophysiological recordings of single protein channels in a model membrane allow investigation of the dynamic properties of the single channel in its native conformation. In the present experiment the electrophysiological properties of the bacterial membrane protein SecYEG were addressed.

2.2 Data acquisation

Figure 1 shows typical cutouts of the current recording with a sampling frequency of 10kHz of single or multiple channel activity at a constant voltage of 50 mV with $\approx$ 20ms duration. In the left panel of Fig. 1 a typical phase is shown, where channel activity was observed, whereas the right panel shows mere background noise, as the ion pores were not inserted yet into the membrane. In total, the experiment consists of two phases of 1 minute each. In the first phase, only background noise is observed. Then, after addition of the protein pores, membrane currents are recorded. During the latter phase, intervals of high channel activity as given in the example and intervals when only background noise was present were recorded. The *solid* arrow indicates a phase of background noise whereas the *dashed* arrows depict current peaks of one or multiple active channels whose levels were used in the subsequent

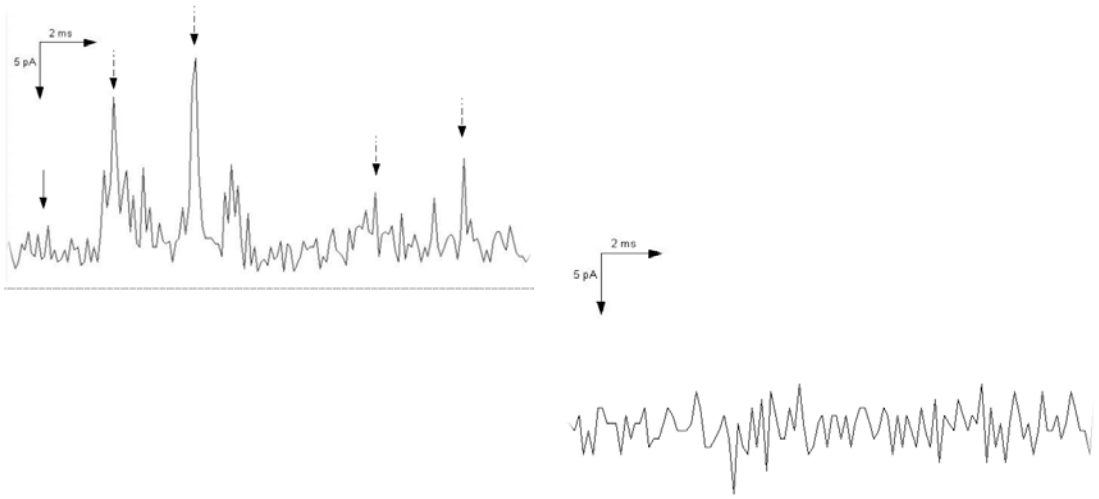

Figure 1: Left: Time dependent recording of the ionic current through SecYEG pores inserted into an artificial lipid membrane of $50\mu m$ diameter at a transmembrane voltage of $50mV$ and 250 millimolar potassium chloride (KCl). The solid arrow indicates a phase of background noise whereas the dashed arrows depict current peaks of one or multiple active channels the levels of which were used in the subsequent analysis. Right: Time dependent recording of background current at a transmembrane voltage of $50mV$ and 250 millimolar potassium chloride (KCl).

analysis.

Here, we analyze a sample of 100 transmembrane currents measured from channel pores that were inserted into an artificial lipid membrane during 10 seconds in the recording of 1 minute. These currents and the background noise levels were

determined from the data as follows.

First, to determine the background noise the baseline was recorded (cf. right panel of Fig. 1 for a cutout of the measurements in this phase) before proteoliposomes (and in consequence channel proteins) were added to the experiment. From this data it is possible to estimate the variance or even the distribution of the noise. Here, we used 1000 measurements to estimate the latter distribution. After adding the protein channels to the experiment, the experimenter chooses the points (peak heights) to be included based on the following rules. The peak has to be above a threshold value, which was 6 pA here, to make the subsequent analysis tractable. The standard method that is used for the selection of the peaks consists of analyzing the data visually. Based on a visual pilot inspection of the data, the experimenter chooses the threshold so that it is significantly smaller than the minimum of all the peaks of interest (e.g. the two right peaks in the left panel of Fig. 1). This implies that some of the single channel current events in the signal are bound to be lost. Thus, it is impossible to use the estimated density of channel current levels to investigate the relative frequency of single vs. multiple channel events. The second rule in the selection of the peaks is that there is a minimal time lag of 1 ms after a peak height was recorded in order to avoid or at least reduce dependency in the data.

2.3 Independence of the measurements

In our subsequent analysis we assume the observed current levels to be an i.i.d. sample of the current level distribution for the following reasons. This assumption can be made because of the nature of the experimental setup. The recording of the single channel currents is not initiated unless a stable (constant) baseline signal has been observed. After the occurrence of a current peak due to a single or

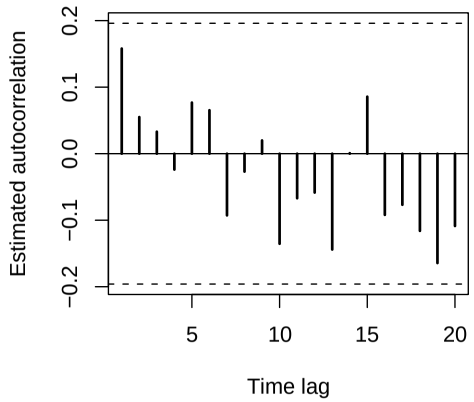

Figure 2: Autocorrelation function of the time series formed by the peak current levels. The dashed, horizontal lines show 95%-coverage probability confidence intervals based on the assumption of an uncorrelated time series.

multiple channel event (i.e. a jump to a new current level) the current returns to the baseline level, which remains stable during the time of recording. On the other hand, the time between two measured channel currents is in general long enough so that it is possible that other random current fluctations or events occur in between. Moreover, the theory of ion pores models the transport of ions via passive diffusion through the central SecYEG pore. No active interaction between the K^+ ions and the SecYEG channel is known up to now. Therefore, it is very improbable that K^+ induces structural changes in the SecYEG molecule during the experiment, which would have barred us from assuming i.i.d. observations. Finally, Fig. 2 shows the autocorrelation function of the observations. Here, we have used the peak level in the temporal order in which they appear in the data, and interpreted this as a time series. The figure provides a strong indication that the data is uncorrelated.

3 Silverman's test for deconvolution

In the preceding section we have argued that in order to understand the biological mechanism on which the ionic flux is based we require tests for certain modality hypotheses of the relevant densities. We will now discuss such a method which is based on an extension of the Silverman test for direct density estimation.

3.1 Monotonicity of the number of modes

Silverman's (1981) test relies on the observation that for a kernel density estimator (or the estimator of a derivative) based on non-noisy observations, the number of modes is a monotonically decreasing, right-continuous function of the bandwidth, if a normal kernel is used. It turns out that this is also true for the deconvolution kernel density estimator (2) based on a normal kernel, as long as it is well-defined. To fix notation, denote the Fourier transform of f by $\Phi_f(t) = \int_{\mathbb{R}} f(x) \exp(itx)\, dx$, and suppose that f is p-times continuously differentiable for some $p \geq 0$. In the sequel suppose that the model $\hat{\psi}$ for the error density is fixed. Under the assumption that $\Phi_{\hat{\psi}}(t) \neq 0$ for all $t \in \mathbb{R}$ and that $\Phi_L(ht)/\Phi_{\hat{\psi}}(t) \in L_1$ for all $h > 0$, the deconvolution kernel density estimator for the j^{th} derivative of f, given by,

$$\hat{f}_n^{(j)}(x; h) = \frac{1}{nh^{j+1}} \sum_{k=1}^{n} K^{(j)}\Big(\frac{x - X_k}{h}; h\Big), \tag{2}$$

where

$$K^{(j)}(x; h) = \frac{1}{2\pi} \int_{\mathbb{R}} (-it)^j \exp(-itx) \frac{\Phi_L(t)}{\Phi_{\hat{\psi}}(t/h)}\, dt \quad 0 \leq j \leq p, \tag{3}$$

exists. Here the smoothing parameter $h > 0$ is called the bandwidth. From now on we let L denote the standard normal kernel, and this kernel will be used in $\hat{f}_n(x; h)$ and in the deconvolution kernel $K^{(j)}(x; h)$. We say that the deconvolution kernel density estimator $\hat{f}_n^{(j)}(x; h)$ with normal kernel is *well-defined* if $t^j \Phi_L(ht)/\Phi_{\hat{\psi}}(t) \in$

$L_2(\mathbb{R})$ for all $h > 0$. One can show that $\hat{f}_n^{(j)}(x;h)$ is well-defined for all ordinary smooth error distributions (for which $\Phi_{\hat{\psi}}(t)$ decays polynomially), as well as for most supersmooth error distributions (for which $\Phi_{\hat{\psi}}(t)$ decays exponentially) such as t-distributions or symmetric stable distributions with self-similarity index $\alpha < 2$. For further discussion see Section 3.3.

Let $\nu_j(h)$ denote the number of modes (i.e. of local maxima) of the deconvolution kernel density estimator $\hat{f}_n^{(j)}(x;h)$ on the real line $\mathbb{R}$ for a fixed bandwidth h.

Theorem 1. *Suppose that the deconvolution density estimator $\hat{f}_n(x;h)$ based on a normal kernel is well-defined. Then $\nu_j(h)$ is a monotonically decreasing and right-continuous function of the bandwidth h with values in $\mathbb{N} \cup \infty$.*

Remark 1. Without additional assumptions on the error distribution, the deconvolution kernel density estimator (2) can have infinitely many modes. For some examples see Balabdaoui et al. 2009. Even if the deconvolution kernel density estimator has infinitely many modes in $\mathbb{R}$, simulations indicate that it typically admits only finitely many modes on a compact interval. Nevertheless, this is no direct solution since if attention is restricted to a finite interval I, Theorem 1 no longer applies, and the number of modes of $\hat{f}_n^{(j)}$ on I need not be monotone any more. However, Hall and York (2001) show in the context of direct density estimation that this causes no serious practical problems, since a. the position of modes can be easily monitored, and thus one sees if a mode leaves the interval I causing non-monotonicity, and b. the probability of having non-monotonicity converges to zero, and hence the problem disappears asymptotically. Similar results could also be derived in the deconvolution setting. However, we shall simply ignore the possible non-monotonicity problem of the number of modes on subsets $I \subset \mathbb{R}$.

3.2 Bootstrapping the critical bandwidth

In the following, we restrict our attention to the estimator $\hat{f}_n^{(0)}(\cdot, h) = \hat{f}_n(\cdot, h)$ of the density f itself. For an interval $I \subset \mathbb{R}$, set

$$h_{crit,m} = \inf\{h : \hat{f}_n(x; h) \text{ has precisely } m \text{ modes in } I\}, \tag{4}$$

which is, as mentioned above, always well-defined if $I = \mathbb{R}$ and the number of modes of the estimator $\hat{f}_n(\cdot, h)$ is finite. In order to assess significance for testing the hypothesis

$$H_m : f \text{ has at most } m \text{ modes} \qquad \text{against} \qquad K_m : f \text{ has more than } m \text{ modes}$$

Silverman (1981) proposed to use the smoothed bootstrap, based on the critical bandwidth $h_{crit,m}$. In our setting, the smoothed bootstrap proceeds as follows.

(i) Sample $\{X_1^*, \ldots, X_n^*\}$ i.i.d. from the density $\hat{g}_n(\cdot; h_{crit,m}) = \hat{f}_n(\cdot; h_{crit,m}) * \hat{\psi}$.

(ii) Compute the kernel estimator, $\widehat{f}_n^*(x; h^*)$ based on the bootstrap data $\{X_1^*, \ldots, X_n^*\}$ and determine the corresponding bootstrap critical bandwidth $h^*_{crit,m}$.

Note that $\hat{g}_n(x; h_{crit,m})$ is just a kernel density estimate of g based on the observations $X_1, \ldots, X_n$, with normal kernel and bandwidth $h_{crit,m}$, the m-critical bandwidth of $\hat{f}_n$. Silverman originally proposed a slight variation of the smoothed bootstrap, in which the sampling density for the bootstrap data is renormalized to have variance equal to the sample variance. One can also give a variant of this procedure in the deconvolution setting, which we however omit for brevity. Using either bootstrap procedure, the hypothesis H_m is rejected with nominal level α if $h_{crit,m}$ is above the $(1-\alpha)$-quantile of the distribution of $h^*_{crit,m}$, i.e. if

$$P\big(h^*_{crit,m} \leq h_{crit,m} | X_1, \ldots, X_n\big) \geq 1 - \alpha. \tag{5}$$

3.3 Choosing the error density

Suitable parametric models for error densities are scale families of the form

$$\psi_\sigma(x) = \psi_0(x/\sigma)/\sigma, \qquad \sigma > 0, \tag{6}$$

where ψ_0 is some standardized reference density. If (as is the case in our application) additional data on the noise are available, the scale parameter σ can be easily estimated. Denote this estimator by $\hat{\sigma}$, then $\hat{\psi} = \psi_{\hat{\sigma}}$. Relevant special cases for ψ_0 are the standard normal density, the standardized Laplace density or the family of standardized t-densities. Meister (2004) gives some theory for deconvolution with misspecified error density, and in particular considers interchanging Laplace and normal density. Here, the Laplace error turns out to be somewhat more robust to misspecification then normal errors.

We note that the estimator (2) is not well-defined for normal errors if the normal kernel is used. Thus, our method cannot be applied with the normal distribution as error model. In mitigation, it can be used with t-distributed errors, which for high degrees of freedom provide accurate approximations to the normal distribution. Further, it can also be applied with nonparametric models for the errors (see Section 4).

3.4 Asymptotic calibration of Silverman's test for unimodality

It is known that Silverman's test is conservative, even asymptotically. Therefore, following Hall and York (2001), we discuss in this section how to calibrate Silverman's (1981) test for unimodality in the case of noisy observations. The theory only applies to ordinary smooth noise, i.e. $\Phi_\psi(t)t^\beta \to c$, $t \to \infty$ for $\beta > 0$, $0 \neq c \in \mathbb{C}$.

However, at least in finite samples, our simulations indicated that the main effect of the error on the results of Silverman's test is its scale (as long as the error density remains unimodal), and not so much the smoothness of the error density.

First assume that ψ is fixed an known. Hall and York (2001) observed that the test decision based on (5) would be (asymptotically) valid if $U_n = P\big(h^*_{crit,1} \leq h_{crit,1} | X_1, \ldots, X_n\big)$ were asymptotically uniformly distributed under the hypothesis H_1, which is, however, not exactly the case. Indeed, the stochastic process $\hat{G}_n(\lambda) = P\left(h^*_{crit,1}/h_{crit,1} \leq \lambda | X_1, \ldots, X_n\right)$ converges weakly to the limiting process $\hat{G}_{\beta,c}(\lambda)$ (cf. the Appendix for the explicit form of $\hat{G}_{\beta,c}(\lambda)$). Note that this limiting process does not depend on the unknown density f, although it depends on the known error density through β (and at a first glance c). Now, since the realizations of $\hat{G}_{\beta,c}(\lambda)$ are continuous, strictly increasing distribution functions, for each $\alpha > 0$ there is a unique $\lambda_{\alpha,\beta,c}$ such that

$$P\big(\hat{G}(\lambda_{\alpha,\beta,c}) \geq 1 - \alpha\big) \leq \alpha.$$

In Corollary 4 in the Appendix we show that $\hat{G}_{\beta,c}(\lambda) = \hat{G}_{\beta,c/|c|}(\lambda)$ and hence that $\lambda_{\alpha,\beta,c} = \lambda_{\alpha,\beta,c/|c|}$ does not depend on the scale parameter of the error distribution. Thus, the quantity $\lambda_{\alpha,\beta,c} = \lambda_{\alpha,\beta,c/|c|}$ required to calibrate Silverman's (1981) test for unimodality for deconvolution needs only to be computed for one member from a scale family. If $c \in \mathbb{R}$ (which is the case for symmetric errors), we simply write $\lambda_{\alpha,\beta}$ for $\lambda_{\alpha,\beta,1}$ or even λ_α if the error density is clearly specified. Once $\lambda_{\alpha,\beta,c}$ is determined for the specific error density in use, the hypothesis H_1 is rejected with asymptotic level $\alpha > 0$ if

$$P\left(h^*_{crit,1}/h_{crit,1} \leq \lambda_{\alpha,\beta,c} | X_1, \ldots, X_n\right) \geq 1 - \alpha.$$

The quantity $\lambda_{\alpha,\beta,c}$ will in practice be determined using simulations, as we shall illustrate in Section 5.

If $\hat{\psi} = \psi_{\hat{\sigma}}$ is estimated within a scale family which satisfies Assumption B' (in the Appendix), and if $\hat{\sigma}$ is consistent (as $n \to \infty$) and independent of the X_i (e.g. estimated from additional data on the noise), then the above asymptotics remain true (cf. Corollary 5 in the Appendix).

4 Results from the analysis of the SecYEG data

In this section we apply the Silverman test for deconvolution introduced in Section 3 to the SecYEG data. The measurements of the current levels X_i are modeled by (1). We consider three different models for the distribution of the noise terms ε_i, the Laplace distribution, the t-distribution with 25 degrees of freedom as well as a nonparametric model. The variance of the Laplace distribution is estimated from the additional observations consisting of background noise, whereas the t-distributed noise is adjusted to have the same variance as the Laplace distribution. The nonparametric model is essentially the empirical distribution function of the noise.

Fig. 3 indicates that both the Laplace and $t-$ densities are not able to fully reproduce the empirical distribution of the noise terms, and a Kolmogorov-Smirnov test for these parametric forms (as well as for normally distributed noise) rejects with p-value < 0.01.

Therefore, we also use the deconvolution estimator by Neumann (1997, eq. 2.7) given by

$$\hat{f}_{n,NP}(x;h) = \frac{1}{2\pi} \int \exp(-itx) \Phi_L(ht) \frac{\widehat{\Phi}_X(t)}{\widehat{\Phi}_\psi(t)} 1_{\{|\widehat{\Phi}_\psi(t)| \geq N^{-1/2}\}} \, dt.$$

where N denotes the length of the baseline series (i.e. $N = 1000$), and $\widehat{\Phi}_\psi(t)$ is the empirical characteristic function of the baseline. Thus, except for the truncation

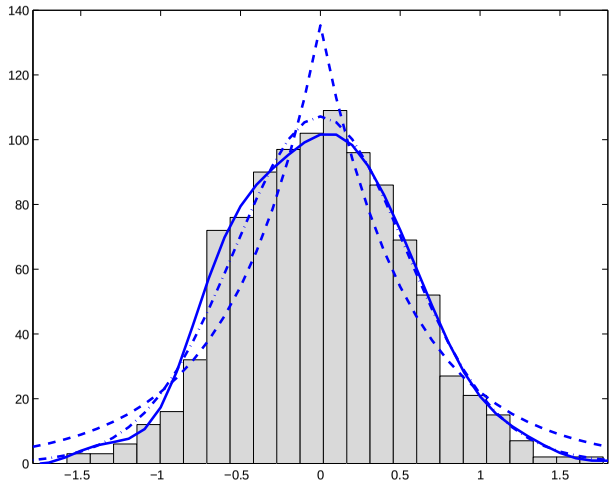

Figure 3: Parametric and nonparametric estimates of the density of the error terms ε_i. Solid line: nonparametric kernel density estimate, dashed: density of a Laplace distribution with the same variance as the observed noise terms, and dash-dotted: density of a t-distribution with 25 degrees of freedom and the same variance as the observed noise terms.

of frequencies lower than $N^{-1/2}$, the characteristic function of the empirical distribution of the noise is used as noise model. One can easily show that for a fixed estimate $\widehat{\Phi}_\psi(t)$, monotonicity of the modes as stated in Theorem 1 still holds true for $\hat{f}_{n,NP}(x;h)$.

It turns out that the finite sample results for the deconvolution density estimator with these three distinct models for the error density do not differ much, the main feature of the noise (at least for finite samples) seems to be the correct specification of the error's standard deviation.

Graphical analysis of the data. Fig. 4 shows the critical density estimates for one, two and three modes for $\hat{f}_{n,NP}(x;h)$. The corresponding estimates based on Laplace and t-distributed noise (not displayed) are very similar. The first, second

and third mode for $\hat{f}_{n,NP}(x;h)$ with bandwidth $h_{crit,3}$ are located at $(11.2, 23.7, 36.9)$. Similarly, for the $t-$distribution based estimate these are located at $(11.3, 22.9, 36.9)$, and for Laplace-distributed noise the modes are at $(11.3, 23.0, 36.9)$. Hence, the estimated locations of the modes are insensitive to the assumptions on the underlying density and appear to be located close to $\approx$ 12pA, $\approx$ 24pA and $\approx$ 36pA, i.e. with an approximately fixed difference of 12pA between the peak locations. This regularity hints at the existence of several, i.e. 2 or 3, protein pores, being responsible for the modes at $\approx$ 24pA and $\approx$ 36pA rather than subconductance states of a single pore. In consequence, a peak of approximately $12pA$ in the density of current levels under the present conditions indicates the presence of a single open protein pore in the membrane.

Testing for the number of modes. We now apply Silverman's test for deconvolution. For the test for unimodality we use the calibrated version with the values λ_α obtained for $n = 100$ in our simulation study in Section 5. For testing two versus three or more modes, the asymptotic distribution of the bootstrap test statistic depends on the true underlying density, and we therefore use the uncalibrated test. For all three models of the error density we get the following results. The calibrated version of Silverman's test for deconvolution with test level 5% rejects the null hypothesis of unimodality, thus providing support for the existence of, at least, one significant secondary mode. Here, the interval of interest I, which determines where modes of the density are searched for, was $[10, 60]$. For details on the selection of I and the determination of the calibration constants λ_α we refer to Section 5. We also tested the null hypothesis of ≤ 2 modes against the alternative of at least 3 modes. Again, the null hypothesis is rejected at a level of 5%. Finally, we tested the null hypothesis of ≤ 3 modes against the alternative of more than three modes which is *not* rejected by the Silverman test for deconvolution.

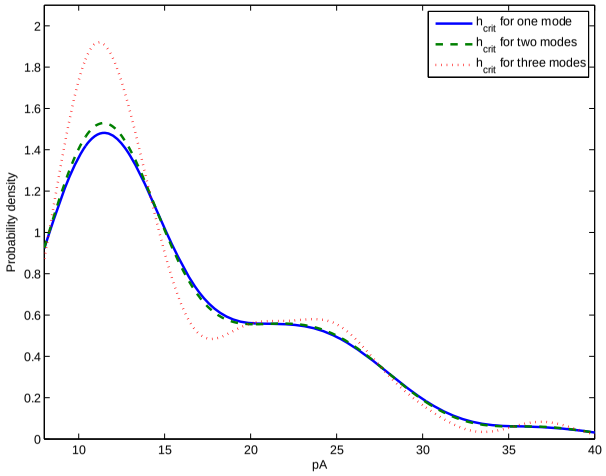

Figure 4: Estimates of the density of ionic current levels through SecYEG, corresponding to the critical bandwidth for one mode (solid line), two modes (dashed line) and three modes (dotted lines). For the deconvolution we use the non-parametric estimator $\hat{f}_{n;NP}(x;h)$ (Neumann, 1997); see text for details.

5 Numerical performance of Silverman's test for deconvolution

Here we report the results of a simulation study for Silverman's test for deconvolution. To this end, we discuss the performance of the original version of Silverman's test for deconvolution, as well as its calibrated version introduced in Section 3.4.

5.1 Simulation results for Laplace-distributed error

We generate observations $X_1, \ldots, X_n$ from model (1) using sample sizes $n = 100$ and $n = 1000$. For assessing the level of the test, we use two unimodal densities for f, and for assessing the power we use a bimodal and a trimodal density. A summary of

Distribution			Interval I
Normal	f_1	$\exp(-x^2/2)/\sqrt{2\pi}$	$[-2, 2]$
Gamma	f_2	$x \exp(-0.15x)\, 0.15^2\, 1_{x\geq 0}(x)$	$[-0.1, 0.9]$
Uniform	f_3	$1_{[0,1]}(x)$	$[-0.1, 1.1]$
Bimodal	f_{bi}	$\frac{e^{-\frac{(x-0.4)^2}{2\cdot 0.05}} + e^{-\frac{(x+0.4)^2}{2\cdot 0.05}}}{\sqrt{8\cdot 0.05\cdot\pi}}$	$[-0.7, 0.7]$
Trimodal	f_{tri}	$\frac{e^{-\frac{(x-0.4)^2}{2\cdot 0.01}} + e^{-\frac{(x+0.4)^2}{2\cdot 0.01}} + e^{-\frac{(x-0.1)^2}{2\cdot 0.01}}}{\sqrt{18\cdot 0.01\cdot\pi}}$	$[-0.6, 0.6]$

Table 1: Densities used to generate the data in the simulations. The last column gives the interval I on which the number of modes in an estimate $\hat{f}_n$ is counted.

the densities f considered is given in Table 1, and Fig. 5 shows the bi- and trimodal densities f_{bi} and f_{tri}. Furthermore, in this section we use a Laplace distributed noise $\psi(x) = \lambda \exp(-\lambda \cdot |x|)/2$ with parameter $\lambda = 3$ (and variance 2/9), which satisfies Assumption B in the Appendix.

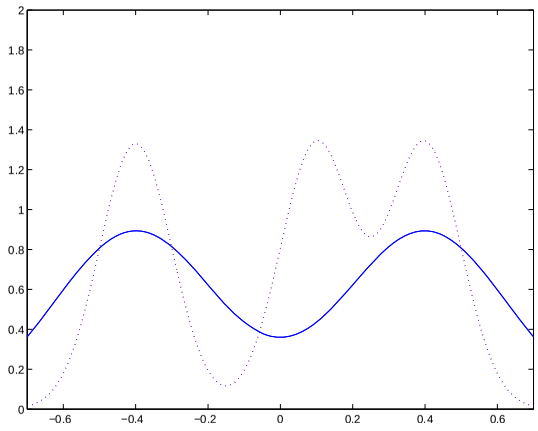

Figure 5: Bimodal and trimodal test densities f_{bi} and f_{tri} used in the power simulations of the Silverman's test(s) for deconvolution.

As already observed by Hall and York (2001) for direct observations, the estimator will have spurious modes in regions where f is small, and for deconvolution the situation is typically even worse. Thus, computing the critical bandwidth in (4) over $I = \mathbb{R}$ is not feasible, and one should restrict attention to a compact interval where $g \geq c > 0$. Table 1 gives details on the intervals I used in the subsequent simulations for the various densities f_i considered.

We use the smoothed bootstrap method suggested in Section 3.2 with 100 bootstrap replications in each simulation run, and, except if noted otherwise, we performed 100 simulations for each combination of test version, sample size, error distribution and underlying density f_i. As a first illustration, estimates with bandwidths $h_{crit,m}$, $m = 1, 2, 3$ based on random samples of size $n = 1000$ for the different target densities f_i are shown in Fig. 6.

Sample size, λ_α	Density/test region/level								
	Normal / $[-2, 2]$			Gamma / $[-0.1, 0.9]$			$U[0, 1]$ / $[-0.1, 1.1]$		
	20%	10%	5%	20%	10%	5%	20%	10%	5%
100, classical	2%	1%	0%	5%	2%	0%	45%	21%	13%
1000, classical	10%	6%	2%	9%	3%	1%	19%	11%	3%
100, λ_α from f_1	22%	10%	5%	21%	9%	4%	15%	5%	3%
1000, λ_α from f_1	19%	11%	6%	11%	7%	5%	34%	22%	12%
100, λ_α from f_2	31%	19%	16%	21%	9%	4%	23%	13%	9%
1000, λ_α from f_2	22%	7%	4%	19%	10%	5%	22%	14%	10%

Table 2: Level of the classical and calibrated version of Silverman's test for deconvolution. The first and second rows correspond to the classical test, the third and fourth rows to the calibration values λ_α based on simulations from the normal density f_1, and the fifth and sixth rows to those based on simulations from the Gamma density f_2.

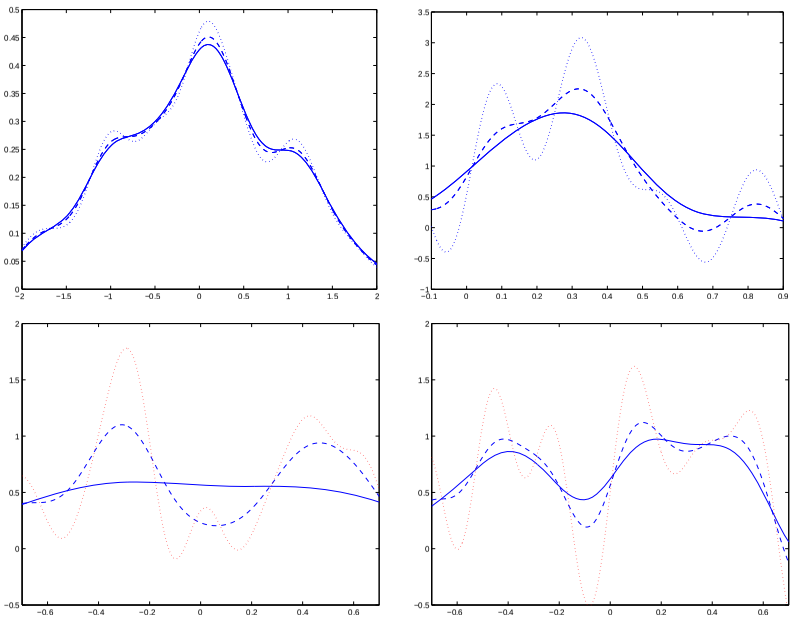

Figure 6: Estimates corresponding to the critical bandwidth for randomly chosen samples of size 1000 from the Gaussian density f_1 (upper left), the density of a Gamma distribution f_2 (upper right), the bimodal density f_{bi} (lower left), and the trimodal density f_{tri} (lower right), respectively. Solid lines correspond to the critical density for one mode, dashed lines for two modes, and dotted lines for three modes, respectively, for all plots except the lower right one. In the latter case, i.e. for the trimodal density f_{tri}, the respective lines correspond to two, three and four modes.

We now discuss the results of simulations of the original Silverman's test for deconvolution, where we test the hypothesis H_1 of unimodality of f on I. The first and second rows of Table 2 give the actual levels of the test for the unimodal target densities f_1 and f_2. The test performs very poorly for the sample size $n = 100$, and is still rather conservative for $n = 1000$. The results for power simulations are shown in the first and second rows of Table 3 where f_{bi} and f_{tri} are used as alternatives. The

Sample size, λ_α	True density f/Level					
	Bimodal			Trimodal		
	20%	10%	5%	20%	10%	5%
100, classical	24%	2%	1%	16%	2%	0%
1000, classical	72%	53%	34%	30%	17%	4%
100, λ_α from f_1	45%	29%	15%	33%	18%	5%
1000, λ_α from f_1	73%	64%	52%	47%	38%	16%
100, λ_α from f_2	42%	34%	30%	36%	25%	15%
1000, λ_α from f_2	80%	71%	60%	85%	75%	61%

Table 3: Power of the classical and calibrated version of Silverman's test for deconvolution for rejecting unimodality, the null hypothesis H_1, whereas the true density f is bimodal resp. trimodal. The first and second rows correspond to the classical test, the third and fourth rows to the calibration values λ_α based on simulations from the normal density f_1, and the fifth and sixth rows to those based on simulations from the Gamma density f_2.

test has no significant power for $n = 100$, but performs reasonably well for $n = 1000$.

Next we investigate the calibrated Silverman's test for deconvolution. First, we determine the calibration values λ_α. This is a computationally demanding task, since a large number of deconvolution density estimators (for each artificial dataset and bootstrap replication) has to be computed in order to achieve a sufficient precision of λ_α. Here, to determine the values of λ_α for a given combination of underlying density f and sample size, we used 50 artificial data sets and 100 bootstrap replications. Table 4 gives the results for λ_α from these calibration runs with the unimodal densities f_1 and f_2.

Sample size	Density/test region/level					
	Normal / $[-2, 2]$			Gamma / $[-0.1, 0.9]$		
	20%	10%	5%	20%	10%	5%
100	1.11	1.13	1.15	1.12	1.16	1.22
1000	1.03	1.07	1.08	1.08	1.09	1.10

Table 4: Calibration values λ_α. The calulations were based on the unimodal densities of a normal and Gamma distribution for samples sizes 100 and 1000. See text for details.

Simulations were then performed in order to assess the rate of rejection of the test under the null hypothesis H_1 of unimodality. Here, two scenarios are possible: The density f may be taken to be the same as the one used to determine the λ_α's, or it might be a different density. Asymptotically, this has no effect, but as can observed, it has an effect for finite samples.

Rows three to six of Table 2 show our results. In particular for the sample size $n = 1000$ the simulated rejection rates are in most cases as close to their nominal levels as we can expect for an *estimate* of the rate of rejection from 100 simulations. Moreover, for the Gaussian and Gamma distribution f_1 and f_2 they are in particular significantly closer than for the classical version of the test. However, the simulations with a uniform density f yield a slightly larger rejection rate, which is due to the fact that this density represents a borderline case between a unimodal and a multimodal density.

Finally, rows three to six of Table 3 shows the result of simulations of the power of the calibrated Silverman's test for deconvolution against the bi- and trimodal alternatives f_{bi} and f_{tri}, i.e. against the same alternatives used in the simulations of the classical test given in the first and second rows. By comparing these results, one

	Density/test region/level								
Sample size	Normal / $[-2,2]$			Gamma / $[-0.1,0.9]$			$U[0,1]$ / $[-0.1,1.1]$		
$n = 1000$	20%	10%	5%	20%	10%	5%	20%	10%	5%
Classical test	8%	2%	0%	4%	1%	0%	9%	2%	1%
λ_α from f_1	21%	10%	7%	4%	1%	1%	9%	4%	4%
λ_α from f_2	39%	18%	11%	23%	11%	4%	29%	16%	8%

Table 5: Level of the Silverman's test for deconvolution with a t-distributed noise. The first row gives the levels for the classical test, whereas the second and third rows give the levels for the calibrated test, where the calibration values λ_α were based from simulations from the normal density f_1 and the Gamma density f_2 respectively.

can see that the calibrated test is much more powerful than its classical counterpart in the deconvolution setting.

5.2 Simulations with t-distributed errors

Now we briefly report on simulation results with t-distributed noise with 5 df and scaling parameter $\lambda = \sqrt{2}/\sqrt{15}$. The resulting t-distribution has variance $\sigma^2 = 2/9$ and Fourier transform $\Phi_{t_\nu}(t) = \left(1 + |\sqrt{3}\lambda t| + 3\lambda^2 t^2\right) \exp(-|\sqrt{3}\lambda t|)$. As discussed in Section 3, Theorem 1 applies to the t-distribution, and Silverman's test for deconvolution is in principle applicable. However, the asymptotic theory in Section 7 was only developed for ordinary smooth noise distributions. Nevertheless, we shall apply the calibration method described in Section 3.4, in order to make the results comparable with those obtained with a Laplace-distributed noise.

Tables 5 and 6 show the simulated rejection rates of the test under the null hypothesis, and the simulated power w.r.t. the bimodal and trimodal alternatives f_{bi}

	True density f/level					
Sample size	Bimodal			Trimodal		
$n = 1000$	20%	10%	5%	20%	10%	5%
Classical test	33%	17%	10%	12%	3%	3%
λ_α from f_1	43%	31%	21%	28%	28%	18%
λ_α from f_2	79%	54%	39%	54%	30%	16%

Table 6: Power of the Silverman's test for deconvolution with a t-distributed noise for rejecting unimodality, the null hypothesis is H_1, whereas the true density f is bimodal resp. trimodal. The first row of results gives the powers for the classical test, whereas the second and third row the powers for the calibrated test, where the calibration values λ_α were based on simulations from the normal density f_1 and the Gamma density f_2 respectively.

and f_{tri}, respectively. The sample size in all simulations was taken to be equal to $n = 1000$, and the calibration values λ_α were determined as $\lambda_{0.8} = 1.02$, $\lambda_{0.9} = 1.033$ and $\lambda_{0.95} = 1.055$ from simulations based on the normal density f_1, and $\lambda_{0.8} = 1.08$, $\lambda_{0.9} = 1.085$ and $\lambda_{0.95} = 1.09$ from simulations based on the Gamma density f_2.
The results for the t-distributed noise and Laplace-distributed noise are rather similar. However, the test based on the t-distributed noise appears to be more conservative. In particular, the calibration constants determined from our simulations based on the normal density f_1 (resp. the Gamma density f_2) yielded poorer (in the sense of being more conservative) levels if applied to data generated from the Gamma density (resp. the normal density).

6 Discussion

There are a number of methods for peak detection in the presence of either deterministic or random noise, e.g. wavelet-based methods (Klann et al. 2007), general filtering approaches (Nimunkar and Tompkins 2007), or methods based on fast Fourier transform (Zhang et al. 2007). However, these only aim at estimating the peak locations and their heights. In contrast, our method allows to test in the presence of noise whether peaks which are observed in an estimator are indeed present in the underlying signal, or whether they are mere sampling artifacts of the estimator. The approach is based on the Silverman test for direct density estimation. Other methods for direct data, e.g. those by Müller and Sawitzki (1991) or by Fisher and Marron (2001), seem not to carry over in a straightforward fashion to noisy observations.

In this paper, we have demonstrated that we are able to discriminate different modes of ionic currents, which indicate the number of open channel proteins in the lipid membrane. The nearly equidistant location of the peaks in the current level distribution for the present experiment supports the notion that they can be assigned to multiple open SecYEG channels in the membrane. In contrast, observations of Wirth et al. (2003) on the eukaryotic homologue of SecY, the Sec61 protein, showed the presence of several subconductance states for a single membrane channel.

Further experiments will be required to dissect the transport properties of the SecYEG channel in artificial lipid bilayers in a more detailed manner. This includes analysis of peptide translocation through the SecYEG pore in native bacterial membranes in combination with the ATPase SecA. A combination of single channel current recording and simultaneous fluorescence imaging gives the possibility to closely monitor the interaction of the protein pore with a fluorescently labelled substrate

(Hemmler et al., 2005). Transporters and ion channels also play an essential role as targets for drugs in diseases of the central nervous system, the cardiac system, and metabolic misfunctions. Single channel recordings allow the characterization of drugs with their target receptor on a nanoscale level and with high throughput which makes the method applicable for drug screenings in pharmaceutical research. For specific commercial biological and pharmaceutical applications of membrane transporters, ion channels and cellular signal transmission cf. e.g. `www.iongate.de` and `http://www.signalomics.com/en/`.

Acknowledgements Kathrin Bissantz gratefully acknowledges financial support of the Volkswagenstiftung, and Nicolai Bissantz acknowledges financial support of the Deutsche Forschungsgemeinschaft, SFB 475. Hajo Holzmann thanks the Claussen-Simon Stiftung and the Landesstiftung Baden-Württemberg, "Juniorprofessorenprogramm", for financial support. The authors would like to thank R. Peters, M. Kahn (CenTech), the associate editor and three anonymous referees for helpful comments.

References

Balabdaoui, F., Bissantz, K., Bissantz, N. and Holzmann, H. (2009) Testing for the number of modes of noisy observations – technical details. Technical report, Bochum University.

Bissantz, N., Dümbgen, L., Holzmann, H. and Munk, A. (2007) Nonparametric confidence bands in deconvolution density estimation. *J. Royal Statist. Society Ser. B.* **69**, 483–506.

Butucea, C. and Matias, C. (2005) Minimax estimation of the noise level and of the signal density in a semiparametric convolution model. *Bernoulli* **11**, 309-340

Carroll, R. J., Hall, P. (1988) Optimal rates of convergence for deconvolving a density. *J.*

Amer. Statist. Assoc. **83**, 1184–1186.

Caviston J. P., Holzbaur E. L. (2009) Huntingtin as an essential integrator of intracellular vesicular trafficking. *Trends Cell Biol. to appear.*

Cheng, M.-Y. and Hall, P. (1999) Mode testing in difficult cases. *Ann. Statist.* **27**, 1294–1315.

Cramér, Harald and Leadbetter, M. R. (1967) *Stationary and related stochastic processes. Sample function properties and their applications.* John Wiley & Sons, New York.

Danelon, C., Nestorovich, E. M., Winterhalter, M., Ceccarelli, M. , Bezrukov, S. M. (2006) Interaction of Zwitterionic Penicillins with the OmpF Channel Facilitates their Translocation. *Biophys. J.* **90**, 1617–27.

Fan, J. (1991a) On the optimal rates of convergence for nonparametric deconvolution problems. *Ann. Statist.* **19**, 1257–1272.

Fan, J. (1991b) Asymptotic normality for deconvolution kernel density estimators. *Sankhya Ser. A* **53**, 97–110.

Fisher, N. I. and Marron, J. S. (2001) Mode testing via the excess mass estimate. *Biometrika* **88**, 499–517.

Hall, P. and York, M. (2001) On the calibration of Silverman's test for multimodality. *Statist. Sinica* **11**, 515–536.

Hemmler, R., Boese, G., Wagner, R., Peters, R. (2005) Nanopore unitary permeability measured by electrochemical and optical single transporter recording. *Biophys J.* **88**, 4000–4007.

Klann, E., Kuhn, M., Lorenz, D. A., Maass, P. and Thiele, H. (2007) Shrinkage versus deconvolution. *Inverse Problems* **23**, 2231–2248.

Lodish, H., Berk, A., Zipursky, S.L., Matsudaira, P., Baltimore, D., Darnell J.E. (2000) *Molecular Biology of the Cell. 4th edition.* W H Freeman and Company, New York.

Mammen, E., Marron, J. S. and Fisher, N. I. (1992) Some asymptotics for multimodality

tests based on kernel density estimates. *Probab. Theory Relat. Fields* **91**, 115–132.

Meister, A. (2004) On the effect of misspecifying the error density in a deconvolution problem. *Can. J. Stat.*, **32**, 439–449.

Müller, D. W. and Sawitzki, G. (1991) Excess mass estimates and tests for multimodality. *J. Amer. Statist. Assoc.* **86**, 738–746.

Nestorovich, E. M., Danelon, C., Winterhalter, M. and Bezrukov, S. M. (2002) Designed to penetrate: time-resolved interaction of single antibiotic molecules with bacterial pores. *Proc. Nat. Acad. Sci.* **99**, 9789-9794.

Neumann, M. H. (1997) On the effect of estimating the error density in nonparametric deconvolution. *Nonparam. Statist.* **7**, 307–330.

Neves, P., Berkane, E., Gameiro, P., Winterhalter, M. and de Castro, B. (2005) Interaction between quinolones antibiotics and bacterial outer membrane porin OmpF. *Bioph. Chem.* **113**, 123-128.

Nimunkar, A. J. and Tompkins, W. J. (2007) R-peak Detection and Signal Averaging for Simulated Stress ECG using EMD. *Proceedings of the 29th Annual International Conference of the IEEE EMBS Cité Internationale*, Lyon, France. Peters, R. (2003). Optical Single Transporter Recording: Transport kinetics in Microarrays of membrane patches. *Ann. Rev. Biophys. Biomol. Struct.* **32**, 47–67.

Silverman, B. W. (1981) Using kernel density estimates to investigate multimodality. *J. Roy. Statist. Soc. Ser. B* **43**, 97–99.

Silverman, B. W. (1983) Some properties of a test for multimodality based on kernel density estimates. *Probability, statistics and analysis* 248–259, London Math. Soc. Lecture Note Ser., 79, Cambridge Univ. Press, Cambridge.

Stefanski, L. and Carroll, R. J. (1990) Deconvoluting kernel density estimators. *Statistics* **21**, 169–184.

Van den Berg, B., Clemons, W. M. Jr., Collinson, I., Modis, Y., Hartmann, E., Harrison, S. C. and Rapoport T. A. (2004) X-ray structure of a protein-conducting channel. *Nature*

427, 36–44.

Yao, P. J., Zhu, M., Pyun, E. I., Brooks, A. I., Therianos, S., Meyers, V. E., Coleman P. D. (2003) Defects in expression of genes related to synaptic vesicle trafficking in frontal cortex of Alzheimer's disease.' *Neurobiol. Dis.* **12**, 97–109.

Wirth A., Jung M., Bies C., Frien M., Tyedmers J., Zimmermann R. and Wagner R. (2003) The Sec61p is a dynamic precursor activated channel. *Mol. cell* **12**, 261–268.

Zhang, S. Q., Zhou, X., Wang, H., Suffredini, A., Gonzales, D., Ching, W.-K., Ng, M.-K-, Wong, S. (2007), Peak Detection with Chemical Noise Removal Using Short-Time FFT for a Kind of MALDI Data. *First Inter. Symp. Optimization Systems Biology*, Beijing, China, pp. 222–231.

7 Appendix: Some asymptotic theory

We start by extending an asymptotic result of Mammen et al. (1992) for the expected number of modes of $\hat{f}_n(\cdot, h)$ to the case of noisy observations. To this end we need the following assumptions.

Assumptions A. We assume that the true density of the unobserved data, f, is twice differentiable, has a compact support and admits a unique mode. More precisely, we assume the following.

A1 $\exists\ -\infty < t_l < t_u < \infty$ such that f is compactly supported on $[t_l, t_u]$,

A2. f is twice continuously differentiable on (t_l, t_u),

A3. $f'(t_l+) > 0$ and $f'(t_u-) < 0$,

A4. f has exactly one maximum, at z_0, in (t_l, t_u),

A5. $f''(z_0) \neq 0$.

Assumption B. The error density is ordinary smooth, and moreover there are $\beta > 0$, $0 \neq c \in \mathbb{C}$, such that $\Phi_\psi(t)t^\beta \to c$, $t \to \infty$.

Under Assumption B, from the dominated convergence theorem if follows that the kernels $K(x;h) = K^{(0)}(x;h)$ defined in (3), converge to a limit version as $h \to 0$, i.e. $h^\beta K(x;h) \to K_{\beta,c}(x)$, $h \to 0$, where

$$K_{\beta,c}(u) \quad = \quad \frac{1}{2\pi c}\int_0^\infty \exp(-iux)x^\beta \Phi_L(x)\,dx + \frac{1}{2\pi \bar{c}}\int_{-\infty}^0 \exp(-iux)|x|^\beta \Phi_L(x)\,dx.$$

This expression specializes to

$$K_{\beta,c}(u) = \frac{1}{2\pi c}\int_{\mathbb{R}} \exp(-iux)|x|^\beta \Phi_L(x)\,dx$$

if the noise is assumed to have density which is symmetric around 0.

Theorem 2. *Let $N(h)$ be the number of modes of the deconvolution kernel density estimator $\hat{f}_n(\cdot;h)$ based on the Gaussian kernel L. Under Assumptions A. and B. with $c \in \mathbb{R}$, for any sequence of bandwidths h such that $0 < \liminf_{n\to\infty} n^{1/(2\beta)+5)}h < \limsup_{n\to\infty} n^{1/(2\beta)+5)}h < \infty$, we have*

$$EN(h) = 1 + H\left(\frac{\sqrt{nh^{2\beta+5}}\sqrt{2\pi}|c|\ |f''(z_0)|}{\left[\int_{\mathbb{R}}|x|^{2(2+\beta)}|\Phi_L(x)|^2dx\right]^{1/2}\ \sqrt{g(z_0)}}\right) + o(1)$$

where $H(x) = L(x)/x + \int_{-\infty}^x L(t)dt - 1$.

The formula reduces to that of Mammen et al. (1992) in case $\beta = 0$. The rate of convergence, in expectation, is $n^{-1/(2\beta+5)}$ and is thus slower than the $n^{-1/5}$ which occurs for noiseless data.

Next we give the asymptotic distribution of the critical bandwidth $h_{crit,1}$ and of its bootstrap version $h^*_{crit,1}$ based on the smooth bootstrap. To this end, we introduce the processes

$$Z_{\beta,c}(r,s) = \frac{1}{r^{3+\beta}}\int_{\mathbb{R}} K''_{\beta,c}(s+u)W(ru)du, \quad r > 0, s > 0$$

and

$$Z^*_{\beta,c}(r,s) = \frac{1}{r^{3+\beta}}\int_{\mathbb{R}} K''_{\beta,c}(s+u)W^*(ru)du, \quad r > 0, s > 0,$$

where W and W^* are two independent two-sided standard Brownian motions. Furthermore, set

$$\kappa(z_0, \beta) = \left[\frac{g(z_0)}{|f''(z_0)|^2} \right]^{1/(2\beta+5)},$$

$$R_{\beta,c} = \inf\{r > 0 : Z_{\beta,c}(r, s) + s \text{ changes sign exactly once in } -\infty < s < \infty\},$$

and let $S_{\beta,c}$ be the unique point such that $s \mapsto Z_{\beta,c}(R_{\beta,c}, s) + s$ changes sign.

Theorem 3. *Under the Assumptions A. and B., we have for the critical bandwidth $h_{crit,1}$ that*

$$n^{1/(2\beta+5)} h_{crit,1} \xrightarrow{d} \kappa(z_0, \beta)\ R_{\beta,c}.$$

Furthermore, for the ratio $h^*_{crit,1}/h_{crit,1}$ we have that

$$\sup_{\lambda \in (0,\infty)} \left| P\left(h^*_{crit,1}/h_{crit,1} \le \lambda | X_1, \ldots, X_n\right) - P\left(R^*_{\beta,c}/R_{\beta,c} \le \lambda | W\right) \right| \to 0$$

in probability, where

$$\begin{aligned} R^*_{\beta,c} \quad = \quad & \inf \Big\{ r > 0 : Z^*_{\beta,c}(r, s) + r^{-1} R_{\beta,c} Z^*_{\beta,c}(R_{\beta,c}, S_{\beta,c} + R^{-1}_{\beta,c} rs) + r^{-1} R_{\beta,c} S_{\beta,c} + s \\ & \text{changes sign exactly once in } -\infty < s < \infty \Big\}. \end{aligned}$$

Thus, the process $\hat{G}_n(\lambda) = P\left(h^*_{crit,1}/h_{crit,1} \le \lambda | X_1, \ldots, X_n\right)$ converges weakly to the limit process $\hat{G}_{\beta,c}(\lambda) = P\left(R^*_{\beta,c}/R_{\beta,c} \le \lambda | W\right)$.

Corollary 4. *Under Assumptions A. and B., we have $R^*_{\beta,c}/R_{\beta,c} \stackrel{d}{=} R^*_{\beta,c/|c|}/R_{\beta,c/|c|}$. and therefore $\hat{G}_{\beta,c}(\lambda) = \hat{G}_{\beta,c/|c|}(\lambda)$.*

Assumption B'. The error density ψ belongs to a scale family (6) for which there are $\beta > 0$ and $c_0 \in \mathbb{R}$ such that

$$\lim_{t \to \infty} \sup_{C_1 \le \sigma \le C_2} |\phi_{\psi_\sigma}(t) t^\beta - c_0 \sigma^{-\beta}| = 0, \quad \forall\ 0 < C_1 < C_2.$$

Corollary 5. *Under Assumptions A. and B' and if $\hat{\sigma}$ is a consistent estimator for σ as $n \to \infty$ and independent of the X_i, then the conclusions of Theorem 3 remain true.*